Forward-scattering and multiple-scattering sources of errors in UV-visible spectroscopy of microspheres

Azizeh Alidoust Ghatar, Baptiste Auguié, and Eric C. Le Ru*

The MacDiarmid Institute for Advanced Materials and Nanotechnology, School of Chemical and Physical Sciences, Victoria University of Wellington, P.O. Box 600, Wellington 6140, New Zealand

E-mail: eric.leru@vuw.ac.nz

Abstract

Conventional UV/Visible spectroscopy instruments measure the extinction spectrum of solutions in a transmission configuration. Because of the finite (non-zero) acceptance angle in detection, errors due to forward scattering and multiple scattering can be introduced when measuring scattering samples. We here experimentally quantify these errors using polystyrene spheres of different sizes for two representative analytical/research UV/Visible instruments, one based on a single beam diode-array and the other on a double beam scanning configuration. The measured spectra for particles larger than $1\,\mu$m are shown to be different between the two instruments, even at low concentration, and also vary with concentration (in contradiction with Beer-Lambert law). We show that systematic errors in the range $10-40\%$ are common in such measurements. We propose a model accounting for both forward and multiple-scattering errors and demonstrate its agreement with our experimental results. This model could reduce systematic errors in measurements of scattering samples by up to 40%.

Introduction

UV-Visible spectroscopy is commonly used for the routine characterization of nano- and micro-particles, for example to measure the plasmon resonances of metallic nanoparticles,[1–3] to determine the size and concentration of gold and silver nanospheres,[4–7] or to study dielectric nano- and microspheres.[8,9] Dielectric microspheres are important in many applications, including in biology for drug release,[10] as fluorescent tags[11] or as phantoms to mimic the optical properties of tissues,[12] in climate-related aerosol research as a model aerosol to calibrate instruments,[13] or in microcavity research as whispering gallery mode resonators.[14]

The UV/Visible spectrum is typically measured in a transmission geometry where both optical absorption and scattering can affect the transmission. The resulting spectrum is therefore the extinction spectrum (sum of absorption and scattering), although it is often loosely referred to as absorption or absorbance spectrum. For many dielectric particles, this spectrum should also correspond to the scattering spectrum in the visible region as there is typically no absorption above 300 nm. In an ideal transmission instrument, no scattering should be detected and the true extinction would be measured. In practice however, light that is scattered at an angle very close to the forward direction may be within the field of view of the detector, which can introduce an error compared to the ideal extinction (or scattering) spectrum. This problem is particularly important for large particles (typically larger than 3 to 5μm), as the scattering profile dramatically concentrates forward as size increases. This issue has been highlighted and studied early on[15–19] and more recently,[20] including in specific contexts such as ocean[21,22] or blood[23] measurements. Ref.[24] developed a more advanced optical transmission set-up to overcome the problem and recover the true extinction spectrum. This approach is however much less practical than standard UV/Vis for routine characterization, so analytical correction based on theoretical calculations are desirable. These require to compute the radiation profile of the scatterers and are therefore particularly suited to spherical scatterers, where Mie theory can be used. A simple model for these forward-scattering errors was provided in the early studies[15,16] and more

recently refined.[25] In both cases, the multiple-scattering effects are neglected, so the models are only valid in the limit of dilute scatterers but their range of applicability has not been clearly stated. The effect of multiple-scattering was investigated both theoretically and experimentally,[17–19] for example in the context of long-pathlength oceanic measurements[21] but have not been quantified in conventional UV/Vis instruments used for research or analytical chemistry applications.

In this work, we aim to quantify experimentally the importance of these errors for two representative UV/Visible instruments, one single-beam (SB) array-based-detection, and one double-beam (DB) photodiode-detection. We show that the problem is instrument-dependent, and can indeed be non-negligible even for relatively small dielectric spheres ($\sim 1\,\mu$m). It also results in strong deviations from Beer-Lambert law (BLL). The latter cannot be explained by the original models[15,16] as they follow BLL. The refined model of Ref.[25] does not follow BLL, but we here show that it does not agree either with experiments. To explain this, we extend the forward-scattering error model to also include the effect of multiple-scattering (MS) along the lines of the work in Ref.[19] The proposed MS model results in non-negligible changes even at relatively low concentrations. The new model explains all the measurements simply using an instrument-specific detector acceptance angle. These findings have implications for any UV/Visible measurements of particles of size above approx $1\,\mu$m. This work suggests that the measured spectra could be both instrument- and concentration-dependent, resulting in potential errors in, for example, the derived concentration. The model provides a relatively simple method to correct for these effects, if the particle size and refractive index are known approximately.

Methods

UV/Visible spectroscopy. We use two representative UV/Vis spectrometers to illustrate our findings. The first one is a Cary 8454 from Agilent, which is a single-beam (SB) instru-

ment with a photodiode array detector. The second is a UV2600 from Shimadzu, which is a double-beam wavelength-scanning instrument. All measurements are performed using 1cm pathlength Quartz cuvettes from Starna, using ultrapure water as reference.

Polystyrene microspheres. Polystyrene microspheres of diameter from 0.75 μm to 3 μm were purchased from Micromod (Germany), all with a stock concentration of 2.7%. We also used 5 μm PS microspheres from Duke Scientific (USA) with a stock concentration of 1%. Solutions were diluted as needed in ultrapure water. For concentration-dependent measurements, the highest concentration solution was first prepared from the stock, and the lower concentrations were obtained by further dilution.

Mie theory. Mie theory[26] was used to compute the optical properties (extinction, absorption, scattering, and radiation profiles) of the PS spheres. We used the SPlaC package (Matlab codes)[3,27] with a very fine discretization of 2881 angles to ensure convergence of integrals relating to the radiation profile. Numerical integrals were performed using a simple rectangular quadrature. The wavelength-dependent refractive index of water was taken from Ref.,[28] while that of PS is discussed further in the text.

Deviations from Beer-Lambert law and stray light

Fig. 1(a-b) shows the concentration dependence of the UV/Vis spectrum for a non-scattering material, here the dye Eosin B, measured in the two UV/Vis instruments under study: a single-beam (SB) diode-array Cary 8454 and a double-beam (DB) scanning photodiode-dectector Shimadzu UV2600. As expected from standard UV/Vis theory, the measured absorbance $A_m(\lambda)$ at all wavelengths closely follows Beer-Lambert law (BLL), in other words, it varies linearly with concentration. This is most evident when normalizing the spectra with concentration c and path length L ($L = 1\,\mathrm{cm}$ in all our experiments), the normalized absorbance spectra $\bar{A}_m(\lambda) = A_m(\lambda)/(cL)$ shown in Fig. 1(c-d) are identical at low con-

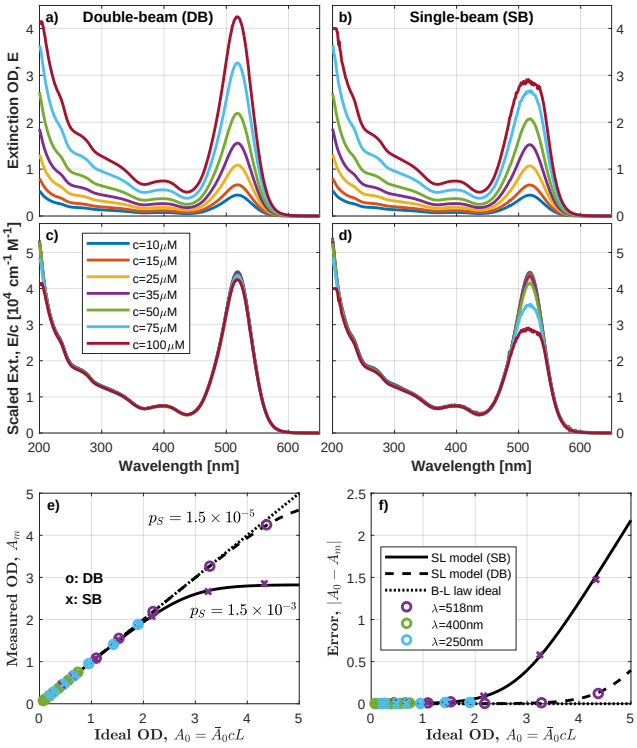

Figure 1: (a-d) UV/Vis spectra of Eosin B dye at different concentrations in two different spectrometers: a DB Shimadzu UV2600 (left) and a SB CCD-array Cary 8454 (right). The spectra are shown as is in the top panels (a-b) and normalized to concentration in the middle (c-d). (e-f) Concentration dependence at selected wavelength: 518, 400, and 250 nm (symbols) showing the deviation from Beer-Lambert law (dotted line, linear). The stray light model for the SB ($p_S = 1.5 \times 10^{-3}$, solid line) and DB ($p_S = 1.5 \times 10^{-5}$, dashed line) show a good agreement with experiments. The measured OD, A_m is plotted against the ideal OD from Beer-Lambert law $A_0 = \bar{A}_0 cL$ in (e) while the error $(A_0 - A_m)$ is plotted in (f). The deviations from BLL are mostly apparent at 518 nm (peak of absorption) where the OD is largest.

centrations and only start deviating at high concentrations. For these low concentrations, $\bar{A}_m(\lambda) = A_m(\lambda)/(cL) = \bar{A}_0(\lambda)$ corresponds to the decadic molar absorption coefficient (in $\mathrm{cm}^{-1}\,\mathrm{M}^{-1}$). Deviations from the Beer-Lambert law can be quantified at a given wavelength λ_0 by considering the error in $A_m(\lambda_0)$, namely $A_m(\lambda_0) - A_0(\lambda_0)$, where $A_0(\lambda_0)$ is the ideal absorption given by $A_0(\lambda_0) = \bar{A}_0(\lambda_0)cL$. As illustrated in Fig. 1(e-f), deviations are observed at the highest ODs for both instruments, but are clearly more pronounced in the SB.

These errors are well understood in terms of stray light. If we denote the stray light probability p_S (defined as a proportion of the incident light intensity), then the predicted OD taking account stray light is (see App. A):

$$A_m = A_0 L - \log_{10}\left[1 + p_S\left(10^{A_0} - 1\right)\right] \tag{1}$$

This stray light model is plotted alongside the experimentally-derived errors in Fig. 1(e-f), from which stray light probabilities of the order of 1.5×10^{-3} (SB) and 1.5×10^{-5} (DB) are derived for these two instruments around 520 nm. Such a difference in stray light is expected between a SB diode-array and a scanning DB spectrometer. The important point in our context is that the stray light errors are negligible up to OD of ~ 2 (SB) or ~ 4 (DB) so we will be able to ignore them in the following.

If we now perform the same experiment on a scattering sample, see Fig. 2 for an example with 3μm polystyrene (PS) microspheres, the results are quite different. Firstly, the non-linear dependence occurs at a much lower OD and cannot therefore be attributed to stray light. Secondly, even in the linear regime (low concentration), the two instruments give noticeably different spectra. The latter can be explained by the fact that some of the forward-scattered light may reach the detector and decrease the apparent extinction, an effect that has been well documented in the past[15,16,22,23,25] and which we revisit in this work.

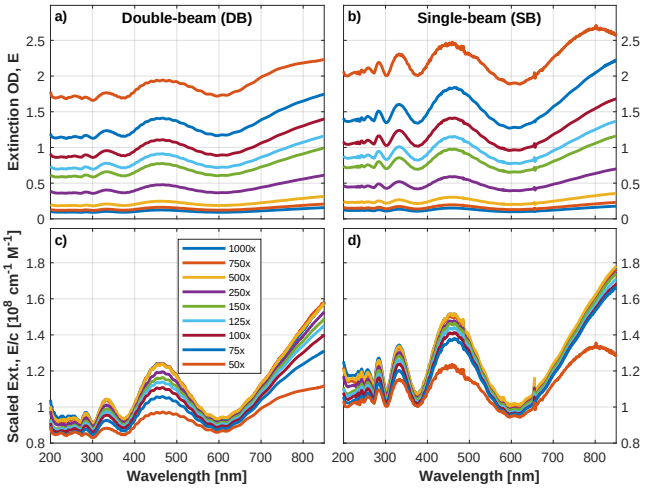

Figure 2: UV/Vis spectra of 3μm-diameter PS spheres at different concentrations in the two different spectrometers: DB (left) and SB (right). The spectra are shown as is in the top panels (a-b) and normalized to concentration in (c-d). Concentrations are indicated as a dilution factor (50× to 1000×) from a stock solution of 2.7% (by mass) polystyrene corresponding to $c \approx 3.4 \times 10^{-12}$ M.

Forward-scattering errors

As illustrated in Fig. 3, particles larger than the wavelength scatter light predominantly forward, and the larger the particle, the more narrow the radiation profile in the forward direction. In a typical UV/Vis instrument, the extinction is measured in transmission mode. An ideal instrument use a perfectly collimated beam and would only measure the transmission of the incident beam, but in practice, light scattered within an acceptance angle Δ of the forward direction will also be detected (Fig. 3(c)). This results in an apparent larger transmission and therefore reduced extinction OD. This effect should be instrument-dependent (through the value of Δ), and particle-size-dependent like the radiation profile. As discussed in previous studies,[15,16,25] forward scattering errors can be quantified for spheres using Mie theory calculations as follows. We first define and calculate the proportion of scattered light that is captured in the detector:

$$p_{\mathrm{det}}(\Delta) = \frac{1}{\sigma_{\mathrm{sca}}} \int_0^{\theta_{\mathrm{det}}} \pi F(\theta) \sin\theta d\theta, \tag{2}$$

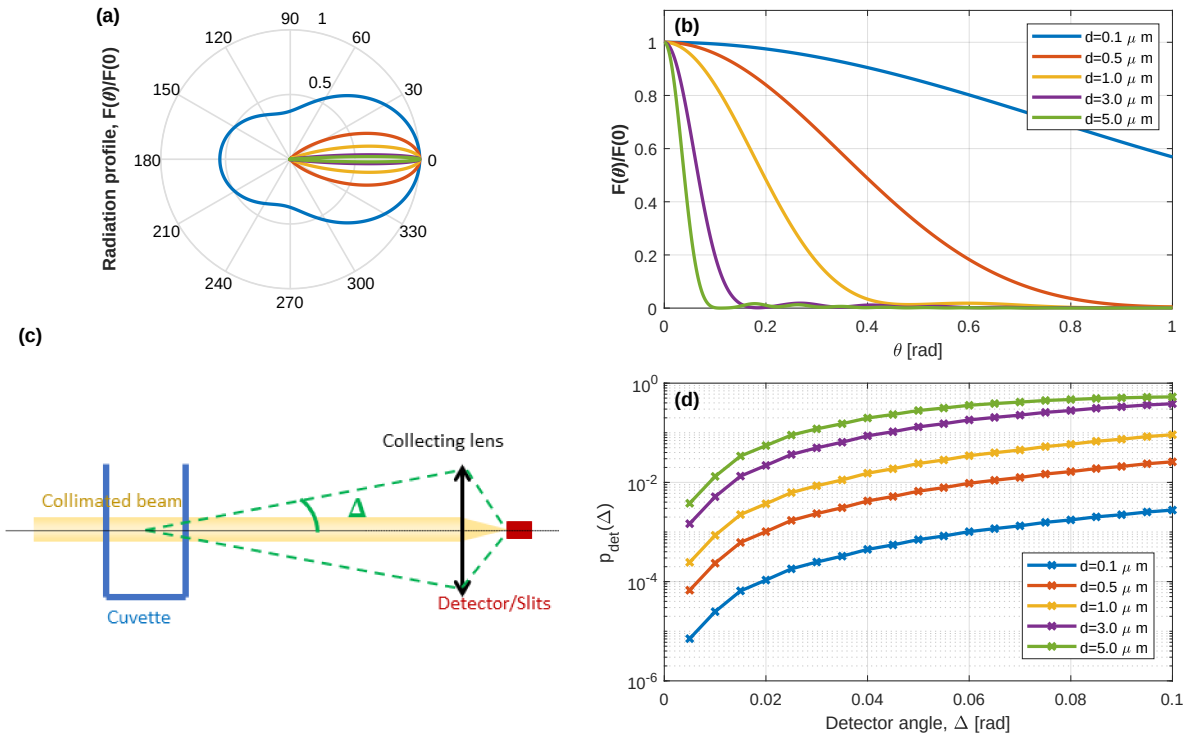

Figure 3: Illustration of forward-scattering errors. The radiation profile, $F(\theta)$ (normalized to 1), computed from Mie theory at $\lambda = 500\,\mathrm{nm}$, is plotted in (a-b) for PS spheres of increasing diameter d immersed in water. The profile becomes increasingly dominated by near-forward scattering. If the detector captures rays scattered within a small acceptance angle Δ (c), then a fraction $p(\Delta)$ of the scattered light will be detected. $p(\Delta)$ can be computed from $F(\theta)$, it increases with Δ and with particle size (d).

where

$$\sigma_{\text{sca}} = \int_0^{\pi} \pi F(\theta) \sin\theta d\theta,$$

is the scattering cross-section and

$$F(\theta) = \frac{\pi}{k^2} \left[S_1(\theta)^2 + S_2(\theta)^2 \right] \tag{3}$$

is the scattering radiation profile for unpolarized light ($k = 2\pi/\lambda$, S_1 and S_2 are the standard scattering amplitudes from Mie theory[26]). Note that in Eq. 2, a circular acceptance area for the detector is assumed to simplify the calculation. This will be appropriate in many cases where a circular lens (or mirror) is used to focus the collimated beam on the detector slits. However, there may be situations where a rectangular mirror or the rectangular slits of the detector determine the acceptance area. In such cases, Eq. 2 should be adapted to the specific geometry, but we expect the additional correction to be small compared to the overall forward-scattering error. Note also that given the rotational symmetry of the problem around the optical axis, the polarization of the incident beam does not affect the final result for p_{det}. Although the expressions above are given for unpolarized illumination for simplicity, the same result would be obtained for polarized light.

In most cases, the measured scatterers are in a solvent (typically water) but the detector is in air, so to account for refraction at the cuvette interfaces, the integral is taken up to angle[16,25]

$$\theta_{\text{det}} = \text{asin}\left(\frac{1}{n_w(\lambda)} \sin(\Delta) \right) \tag{4}$$

rather than Δ. n_w is the refractive index of the solvent, typically water, which may be wavelength-dependent. We also note that when computing numerically the integral in Eq. 2, a fine quadrature is necessary to properly capture the narrow profile, especially for larger

particles. Some representative results of this approach are shown in Fig. 3(d). Even at relatively small Δ, for example $\Delta = 0.04\,\mathrm{rad} \approx 2.3\,^\circ$, p_{det} can reach 10% for particles of $3\,\mu$m diameter or more, which would result in large errors in the measured extinction. It should be noted that this approach applies for a large number of scatterers as in typical UV/Vis spectroscopy. For more advanced experiments with single or a small number of particles, more subtle interference effects between forward scattering and incident beam must be taken into account.[29–31]

Following the model of Ref.,[25] if we denote by I_0 the incident light, the transmitted light in an ideal case should then be $I_t = I_0 \times 10^{-E}$ where $E = A + S$ is the extinction OD (sum of absorption and scattering contributions). The intensity of the scattered light takes the form:

$$I_S = I_0 \frac{S}{E} \left(1 - 10^{-E}\right). \tag{5}$$

Assuming a proportion $p_{\mathrm{det}}(\Delta)$ of this scattered light is detected, the apparent transmitted light is now instead $\bar{I}_t = I_t + p_{\mathrm{det}}(\Delta) I_S$ and the apparent extinction is (here adding the stray light probability p_S to the model):

$$\begin{aligned} E_m &= -\log_{10} \frac{\bar{I}_t}{I_0} \\ &= E - \log_{10} \left[1 + \left(10^E - 1\right) \left(p_S + \frac{S}{E} p_{\mathrm{det}}(\Delta)\right)\right]. \end{aligned} \tag{6}$$

From this, we clearly see that this effect could be much more important than stray light if Δ is not zero, even for small particle size. This model also has a non-trivial concentration dependence deviating from BLL. In the dilute limit, $E \ll 1$ and $10^E \approx 1 + E \ln 10$, so neglecting stray light, we have:

$$E_m \approx E - \log_{10} \left[1 + S(\ln 10) p_{\mathrm{det}}(\Delta)\right] \approx E - S p_{\mathrm{det}} \tag{7}$$

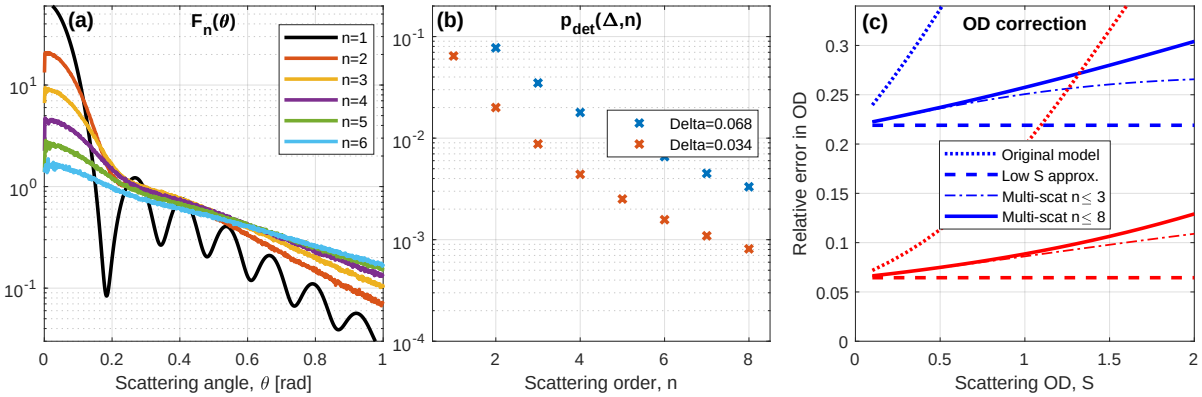

Figure 4: Multiple scattering effects for a 3μm PS sphere at 500 nm. (a) Angular distribution after n scattering events, $F_n(\theta)$. $F_1(\theta)$ is computed from Mie theory and used to iteratively compute $F_n(\theta)$ using Monte-Carlo simulations (see App. B). (b) Probability of forward scattering detection within the acceptance angle Δ (computed from Eq. 2 with the corresponding $F_n(\theta)$). (c) Resulting OD correction, $(E_m - E)/E$ computed from Eq. 10, compared to the original forward-scattering model, Eq. 6. The correct result ($E_m = E$) corresponds to a zero OD correction. The non-zero error at low scattering is due to forward-scattering errors. As in (b), blue corresponds to $\Delta = 0.068$ and red to $\Delta = 0.034$. Note that the particles are non-absorbing here, so $E = S$.

The latter expression corresponds to the original model[15,16] and is linear with concentration as BLL, but note that it is not identical to BLL ($E_m = E$) and exhibit a smaller slope. In this case, for non-absorbing scatterers ($S = E$), the relative error due to forward-scattering is then simply $p_{\mathrm{det}}(\Delta)$ (note that this is a wavelength-dependent function).

Multiple-scattering errors

One major problem with these models is that they ignore the possibility of multiple scattering events, which change the probability distribution of scattered angles.[21] The impact of multiple scattering on transmission measurements in has been well recognized.[32] It can be studied within radiative transfer theory in the small angle approximation, which is valid for particles much larger than the wavelength.[17,18,33] However, for intermediate sizes as considered here, a full calculation based on Monte Carlo ray tracing experiments may be necessary.[19] We note that coherent effects due to particle-particle interaction may also occur at high concentra-

tion,[34–38] but these are ignored here given the relatively low scattering range measurable in conventional UV/Vis systems (with ODs up to 3-4 over a 1 cm pathlength).

To extend the FS model to account for multiple scattering, we here propose a model inspired from a full Monte-Carlo ray tracing simulation of the system,[19] but including a number of simplifications. We first consider separately situations where exactly n scattering events and no absorption occur, the probability of which is given by:

$$p_{\mathrm{sca}}(n) = \frac{(S \ln 10)^n}{n!} 10^{-E} \tag{8}$$

Note that $\sum_{n=1}^{\infty} p_{\mathrm{sca}}(n) = 10^{-A} - 10^{-E}$ is the total probability of scattering only (no absorption), and $p_{\mathrm{Scat}}(n=0) = 10^{-E}$ corresponds to the normal transmission probability. The probability of absorption (including after some scattering events) is $1-10^{-A}$ and those three terms add up to 1, as it should. In an ideal measurement with $\Delta = 0$, scattering events (whether single or multiple) are not detected and only $p_{\mathrm{Scat}}(n=0)$ matters. But when $\Delta > 0$, multiple scattering events change the probability distribution of scattered angles, and $p_{\mathrm{det}}(\Delta, n)$ therefore now depends on n. The transmitted intensity can be expressed as (we here neglect stray light effects):

$$\frac{\bar{I}_t}{I_0} = \sum_{n=0} p_{\mathrm{sca}}(n) p_{\mathrm{det}}(\Delta, n) \tag{9}$$

where $p_{\mathrm{det}}(\Delta, n=0)$=1. If we separate the first term ($n=0$), we can write the measured OD as

$$E_m = E - \log_{10}\left[1 + \sum_{n=1} \frac{(S \ln 10)^n}{n!} p_{\mathrm{det}}(\Delta, n)\right] \tag{10}$$

$p_{\mathrm{det}}(\Delta, n=1)$ is the same as the one introduced in the previous forward-scattering error model and can be computed from the scattering profile from Mie theory, $F(\theta)$, see Eq. 2. If we set $p_{\mathrm{det}}(\Delta, n) = p_{\mathrm{det}}(\Delta, n=1)$, then the sum in the above expression is analytic and we

recover the refined forward-scattering model expression (Eq. 6). This is in fact a pretty bad assumption as illustrated in Fig. 4. After a known number of scattering events, n, we can calculate the modified radiation profile, $F_n(\theta)$, from $F_1(\theta) = F(\theta)$. For this, we used Monte Carlo simulations as explained in App. B. Note that this treatment only considers angles, not any ray/beam position shift, which could affect our ability to detect it in a real optical system (this limitation also applied to the original model).

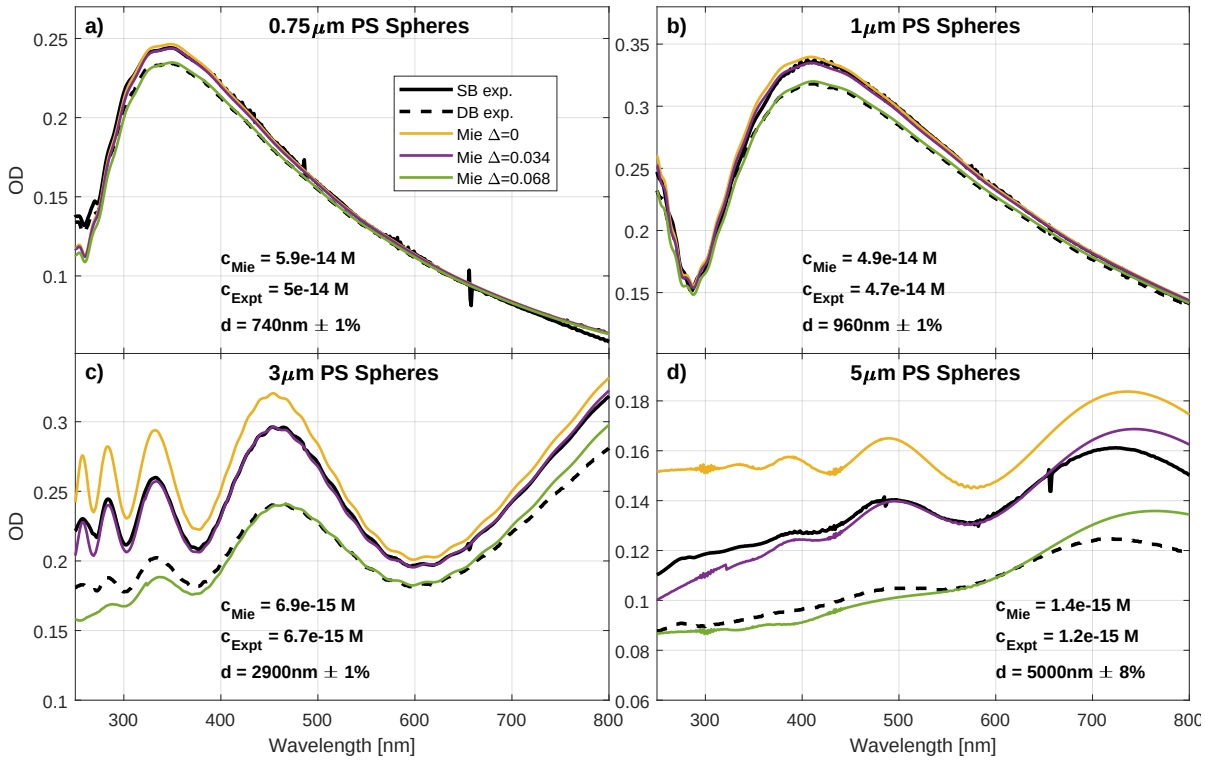

Figure 5: Comparison of experiments and predictions for low concentration extinction spectra of PS spheres in water measured on the single beam (SB, solid lines) and double beam (DB, dashed lines) instruments. The nominal sphere diameters are (a) 0.75, (b) 1, (c) 3, and (d) 5 μm. Mie calculations are carried out for a Gaussian distribution of sizes with mean d and standard deviation σ, indicated in each plot as $d \pm \sigma/d$. Also shown are the concentration used in the Mie results, c_{Mie} and the nominal experimental one c_{Expt}. The Mie predictions are shown as is ($\Delta = 0$) and accounting for forward-scattering errors using Eqn. 7 with $\Delta = 0.034$ (matching the SB data) or $\Delta = 0.068$ (matching DB).

The resulting probability distributions are shown in Fig. 4(a) in the case of 3μm PS spheres at 500 nm. It is clear that the sharp forward nature of the probability distribution

disappears very quickly as n increases, and even for $n = 2$ (note the log-scale in Fig. 4(a)). This results in a sharp decrease of $p_{\mathrm{det}}(\Delta, n)$ with n, see Fig. 4(b). Including multiple-scattering effects dramatically affects the predictions of the model as a function of scattering (or equivalently concentration) as shown in Fig. 4(c). We also see from Fig. 4(c) that high-order scattering must be included to obtain a convergent result in the sum in Eq. 10, for example up to at least $n = 8$ for scattering ODs up to 2. Given the numerical complexity of the full multiple-scattering model, it is desirable to find a suitable approximation, at least for low concentrations/ODs. Figure 4(c) shows that the refined model,[25] Eq. 6 (which assumes $p_{\mathrm{det}}(\Delta, n) = p_{\mathrm{det}}(\Delta, n = 1)$), is a very bad approximation. It deviates substantially from the multiple-scattering result, even at very low concentrations with ODs of the order of $0.1 - 0.2$ only. Paradoxically, the original model, Eq. 7, based on $p_{\mathrm{det}}(\Delta, n \geq 2) = 0$ provides a better approximation than the refined model. Note that it is also the small-OD limit for all models. In practice, one can therefore use this low OD approximation when possible, typically up to ODs of $0.2 - 0.5$ depending on the instrument and the required accuracy.

Comparison with experiments

We can now compare our experimental results to theoretical predictions using the models developed in the previous section. We first start with low-concentration measurements where the results are linear with concentration, typically for ODs smaller than $\sim 0.2 - 0.3$. As just explained, the single-scattering model is incorrect even in this regime, but the low-scattering approximation, Eq. 7, provides a reasonable approximation of the full multiple-scattering model. We therefore use this approximation to compute predicted spectra from Mie theory and compare them to experiments for PS spheres of mominal diameters 0.75, 1, 3, and $5\,\mu$m, see Fig. 5. In each case, we consider a Gaussian distribution of sizes and adjust the mean diameter and standard deviation to match our observed spectra. The predicted spectra are quite sensitive to the average size; less so to the standard deviation, but the latter

does improve agreement (compared to a single size). The derived diameters and standard deviations are consistent with the manufacturer specifications. For the Gaussian distribution, the radiation profile is computed from Mie theory, from which $p_{\mathrm{det}}(\Delta)$ is computed from Eq. 2 for all wavelengths. The acceptance angle of each instrument was adjusted to match experiments resulting in $\Delta = 0.034\,\mathrm{rad} \approx 2°$ for the SB Cary and $\Delta = 0.068\,\mathrm{rad} \approx 4°$ for the DB Shimadzu. This parameter should be the same for all measurements in a given instrument. To match the Mie theory predictions to the measured OD, it is also necessary to apply a scaling parameter related to particle concentration. In all cases, the derived concentration is close to the manufacturer specification, further strengthening the validity of the results. These results are summarized in Fig. 5.

Table 1: Parameters for polystyrene refractive index from Zhang *et al.*[39] and as derived from this work. These two models only differ materially for $\lambda < 400\,\mathrm{nm}$.

-	A	B	C	D
Zhang *et al.*	1.56385	0.007855	0.000315	0
This work	1.56479	0.007357	0.0002454	1.842×10^{-5}

The agreement between predictions and experiments is overall very good, which is notable given the small number of parameters (e.g. a single Δ per instrument for all particle sizes). The substantial change in spectrum due to forward-scattering errors is explained quantitatively by the model across different instruments. Such a good agreement could not be obtained with the existing single-scattering model from Ref.[25] The measured OD can be much smaller than the ideal OD ($\Delta = 0$) for the larger particles. For 5μm particles, the average error is about 16% for the SB instrument ($\Delta \approx 2°$) and 35% for the DB ($\Delta \approx 4°$). These are much larger than one would typically accept in UV/Vis spectroscopy. Even for the smaller $0.75\,\mu$m particles, an error of 5% is obtained at the peak for the DB instrument.

The good agreement between theory and experiment moreover provides a tight constraint on the wavelength-dependence of the refractive index. We initially used the polystyrene refractive index as reported by Zhang *et al.*,,[39] itself very similar to earlier measurements.[40]

It can be analytically modeled as

$$n(\lambda) = A + \frac{B}{\lambda^2} + \frac{C}{\lambda^4} + \frac{D}{\lambda^6} \tag{11}$$

with A, B, C, D given in Tab. 1. Although good agreement was obtained above 400 nm, there were distinct discrepancies below 400 nm across all sizes. These were corrected by changing A, B, C, D as summarized in Tab. 1. These parameters were chosen to keep the refractive index almost unchanged above 400 nm, but it is notably increased below 400 nm to match experiments. We believe this new expression is closer to the actual refractive index of our particles. This discrepancy is not surprising as Ref.[39] only focused on the range above 400 nm. The remaining small discrepancies in Fig. 5, especially at the spectral boundaries for larger spheres, may stem from the approximations we have made. The likely largest remaining source of error is the assumption that the scattered light originates from a point source inside the cuvette. Even if this is approximately justified at low scattering, in the multiple scattering regime, the extent of the illuminating beam could extend beyond its original geometry.[17] This secondary effect could be studied using radiative transfer theory[17] or Monte-Carlo Ray tracing simulations,[19] but this would increase a lot the complexity of the model for a modest gain in accuracy. From the results of Fig. 5, we can estimate that a correction based on the model we presented would reduce these errors to under 5% in the majority of cases.

Finally, to verify our proposed multiple-scattering model, we can also consider the concentration dependence, which as evidenced in Fig. 2 deviates strongly from Beer-Lambert law. The situation is complicated here as the deviation from BLL originates from the forward-scattering error, which is itself affected by multiple-scattering as seen in Fig. 4(c). This results in a non-trivial wavelength dependence. For illustration, we here consider a single wavelength, $\lambda = 460\,\text{nm}$, and focus on the relative error in OD, as compared to the ideal OD $A_0 = \bar{A}_0 cL$, see Fig. 6. Even at low concentration, the error is non-zero and

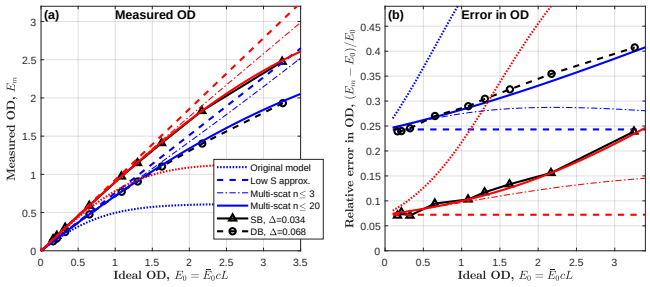

Figure 6: Experimental concentration dependence for $3\,\mu m$ PS spheres at 460 nm showing the deviation from Beer-Lambert law for the SB (triangles) and DB (circles) instruments. The measured OD, E_m is plotted against the ideal OD $E_0 = \bar{E}_0 cL$ in (a) while the relative error $(E_0 - E_m)/E_0$ is plotted in (b). These are compared to different theoretical models with $\Delta = 0.034$ (in red, for SB) or $\Delta = 0.068$ (in blue, for DB): original forward-scattering model (Eq. 6, dotted lines), low-OD approximation (Eq. 7, dashed lines), and multiple-scattering model (Eq. 10, solid lines). The latter is also shown with only three terms in the sum calculated.

given by $1 - p_{\mathrm{det}}(\Delta, n = 1)$ (and therefore particle- and instrument-dependent). The full multiple-scattering model is shown to follow closely the experimentally observed concentration dependence. This is a strong vindication of the model, as no additional free parameters are introduced (Δ was already set from the low-concentration results discussed earlier). In contrast, the original forward-scattering model clearly differs from experiments, even at relatively low concentration. The simple low-scattering approximation is arguably better, but only valid for scattering below ~ 0.3. Fig. 6(b) also shows that the sum in Eq. 10 can be truncated at $n = 3$ for ODs up to ~ 1, but should be evaluated up to relatively large n (we used $n = 20$) to be accurate at the largest ODs.

Discussion and conclusion

These results provide quantitative examples of the potential errors in UV/Vis spectroscopy of scattering samples in conventional instruments. For illustration, these are summarized in Fig. 7, where the expected errors in measured extinction at 500 nm are shown as a function of particle size. Even at low concentrations, these errors can be significant, for example over 10% for $2\,\mu$m particles in the DB instrument we tested. In this regime, the errors are forward-

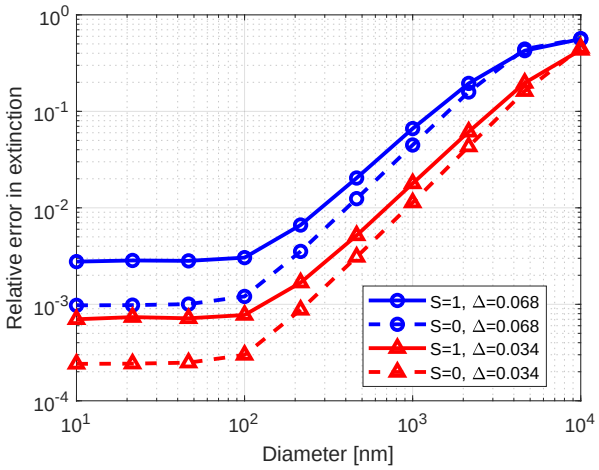

Figure 7: Expected extinction errors as a function of particle size for a purely scattering sample of polystyrene spheres. We assume a fixed wavelength of 500 nm and consider the low-scattering/low-concentration limit (dashed lines) or a sample with a scattering OD of 1 (solid lines). The multiple-scattering model with 20 scattering steps is used in the latter case. We also considered two acceptance angles $\Delta = 0.034$ and $\Delta = 0.068$, corresponding to the two instruments under study.

scattering errors due to the finite acceptance angle of the instrument. Different spectra are therefore measured in different instruments, as we clearly evidenced. At scattering ODs above 0.3, multiple-scattering becomes important and must be accounted for using a more elaborate model. All these errors are under 1% for particle size below 100 nm, but can reach 35% for particles 5 μm and larger. Mie modeling for gold or silver particles (not shown) suggest that the radiation profiles are similar to those of dielectric particles, and similar errors are therefore predicted. The conclusions should also hold at least semi-quantitatively for non-spherical particles.

Given that these corrections are rarely accounted for, any technique/study relying on UV/Vis spectroscopy to characterize particles larger than 1 μm, for example to determine concentration, likely suffers from systematic errors in excess of 10%. The models presented in this work could be used to correct these errors.

Acknowledgement

The authors thank the Royal Society Te Apārangi for support through Marsden grants.

References

(1) Kelly, K. L.; Coronado, E.; Zhao, L. L.; Schatz, G. C. The Optical Properties of Metal Nanoparticles: The Influence of Size, Shape, and Dielectric Environment. *J. Phys. Chem. B* **2003**, *107*, 668–677.

(2) Myroshnychenko, V.; Rodriguez-Fernandez, I., J.and Pastoriza-Santos; Funston, A. M.; Novo, C.; Mulvaney, P.; Liz-Marzan, L. M.; Garcia de Abajo, F. J. Modelling the optical response of gold nanoparticles. *Chem. Soc. Rev.* **2008**, *37*, 1792–1805.

(3) Le Ru, E. C.; Etchegoin, P. G. *Principles of Surface Enhanced Raman Spectroscopy and Related Plasmonic Effects*; Elsevier: Amsterdam, 2009.

(4) Haiss, W.; Thanh, N. T. K.; Aveyard, J.; Fernig, D. G. Determination of Size and Concentration of Gold Nanoparticles from UV-Vis Spectra. *Anal. Chem.* **2007**, *79*, 4215–4221.

(5) Khlebtsov, N. G. Determination of Size and Concentration of Gold Nanoparticles from Extinction Spectra. *Anal. Chem.* **2008**, *80*, 6620–6625.

(6) Grand, J.; Auguié, B.; Le Ru, E. C. Combined Extinction and Absorption UV–Visible Spectroscopy as a Method for Revealing Shape Imperfections of Metallic Nanoparticles. *Anal. Chem.* **2019**, *91*, 14639–14648.

(7) Djorović, A.; Oldenburg, S. J.; Grand, J.; Le Ru, E. C. Extinction-to-Absorption Ratio for Sensitive Determination of the Size and Dielectric Function of Gold Nanoparticles. *ACS Nano* **2020**, *14*, 17597–17605.

(8) Gienger, J.; Bär, M.; Neukammer, J. Extinction spectra of suspensions of microspheres: determination of the spectral refractive index and particle size distribution with nanometer accuracy. *Appl. Opt.* **2018**, *57*, 344–355.

(9) Eneren, P.; Aksoy, Y. T.; Zhu, Y.; Koos, E.; Vetrano, M. R. Light extinction spectroscopy applied to polystyrene colloids: Sensitivity to complex refractive index uncertainties and to noise. *J. Quant. Spectrosc. Rad. Transf.* **2021**, *261*, 107494.

(10) Freiberg, S.; Zhu, X. X. Polymer microspheres for controlled drug release. *Int. J. Pharmaceutics* **2004**, *282*, 1–18.

(11) Kawaguchi, H. Functional polymer microspheres. *Progr. Polymer Sci.* **2000**, *25*, 1171–1210.

(12) Durkin, A. J.; Jaikumar, S.; Richards-Kortum, R. Optically Dilute, Absorbing, and Turbid Phantoms for Fluorescence Spectroscopy of Homogeneous and Inhomogeneous Samples. *Appl. Spectrosc.* **1993**, *47*, 2114–2121.

(13) Chartier, R. T.; E., G. M. Initial investigation of the wavelength dependence of optical properties measured with a new multi-pass Aerosol Extinction Differential Optical Absorption Spectrometer (AE-DOAS). *Atmosph. Meas. Tech.* **2012**, *5*, 709–721.

(14) Chiasera, A.; Dumeige, Y.; Féron, P.; Ferrari, M.; Jestin, Y.; Nunzi Conti, G.; Pelli, S.; Soria, S.; Righini, G. C. Spherical whispering-gallery-mode microresonators. *Laser & Photonics Reviews* **2010**, *4*, 457–482.

(15) Gumprecht, R. O.; Sliepcevich, C. M. Scattering of Light by Large Spherical Particles. *J. Phys. Chem.* **1953**, *57*, 90–95.

(16) Heirwegh, K. P. M. Errors in extinction measurements as due to scattering of light by solutions of relatively small particles. *J. Colloid Interf. Sci.* **1966**, *21*, 1–8.

(17) Tam, W. G.; Zardecki, A. Multiple scattering to the Beer-Lambert law 1: Open detector. *Appl. Opt.* **1982**, *21*, 2405–2412.

(18) Zardecki, A.; Tam, W. G. Multiple scattering corrections to the Beer-Lambert law 2: Detector with a variable field of view. *Appl. Opt.* **1982**, *21*, 2413–2420.

(19) Battistelli, E.; Bruscaglioni, P.; Ismaelli, A.; Lo Porto, L.; Zaccanti, G. Separation and analysis of forward scattered power in laboratory measurements of light beam transmittance through a turbid medium. *Appl. Opt.* **1986**, *25*, 420–430.

(20) Li, X.; Zhao, J. M.; Wang, C. C.; Liu, L. H. Improved transmission method for measuring the optical extinction coefficient of micro/nano particle suspensions. *Appl. Opt.* **2016**, *55*, 8171–8179.

(21) Piskozub, J.; Stramski, D.; Terrill, E.; Melville, W. K. Influence of forward and multiple light scatter on the measurement of beam attenuation in highly scattering marine environments. *Appl. Opt.* **2004**, *43*, 4723–4731.

(22) Boss, E.; Slade, W. H.; Behrenfeld, M.; Dall'Olmo, G. Acceptance angle effects on the beam attenuation in the ocean. *Opt. Express* **2009**, *17*, 1535–1550.

(23) LeBlanc, S. E.; Atanya, M.; Burns, K.; Munger, R. Quantitative impact of small angle forward scatter on whole blood oximetry using a Beer–Lambert absorbance model. *Analyst* **2011**, *136*, 1637–1643.

(24) He, G. S.; Qin, H.-Y.; ; Zheng, Q. Rayleigh, Mie, and Tyndall scatterings of polystyrene microspheres in water: Wavelength, size, and angle dependences. *J. Appl. Phys.* **2009**, *105*, 023110.

(25) Gaigalas, A. K.; Wang, L.; Karpiak, V.; Zhang, Y.-Z.; S.Choquette Measurement of Scattering Cross Section with a Spectrophotometer with an Integrating Sphere Detector. *J. Res. Natl. Inst. Stand. Technol.* **2012**, *117*, 202–215.

(26) Bohren, C. F.; Huffman, D. R. *Absorption and scattering of light by small particles*; John Wiley & Sons Inc.: New York, 1983.

(27) Le Ru, E. C.; Etchegoin, P. G. SERS and Plasmonics Codes (SPlaC). Matlab codes freely available from http://www.vuw.ac.nz/raman/book/codes.aspx (accessed 1st Aug. 2024).

(28) Harvey, A. H.; Gallagher, J. S.; Levelt Sengers, J. M. H. Revised Formulation for the Refractive Index of Water and Steam as a Function of Wavelength, Temperature and Density. *J. Phys. Chem. Ref. Data* **1998**, *27*, 761–774.

(29) Berg, M. J.; Sorensen, C. M.; Chakrabarti, A. Extinction and the optical theorem. Part I. Single particles. *J. Opt. Soc. Am. A* **2008**, *25*, 1504–1513.

(30) Berg, M. J.; Sorensen, C. M.; Chakrabarti, A. Extinction and the optical theorem. Part II. Multiple particles. *J. Opt. Soc. Am. A* **2008**, *25*, 1514–1520.

(31) Mishchenko, M. I.; Berg, M. J.; Sorensen, C. M.; van der Mee, C. V. On definition and measurement of extinction cross section. *J. Quant. Spectrosc. Rad. Transf.* **2009**, *110*, 323–327.

(32) Wang, M. C.; Guth, E. On the theory of multiple scattering, particularly of charged particles. *Phys. Rev.* **1951**, *84*, 1092–1111.

(33) Khlebtsov, N. Role of multiple scattering in turbidimetric investigations of dispersed systems. *J. Appl. Spectrosc.* **1984**, *40*, 243–247.

(34) Bringi, V. N.; Varadan, V. V.; Varadan, V. K. Coherent wave attenuation by a random distribution of particles. *Radio Science* **1982**, *17*, 946–952.

(35) Ishimaru, A.; Kuga, Y. Attenuation constant of a coherent field in a dense distribution of particles. *J. Opt. Soc. Am.* **1982**, *72*, 1317–1320.

(36) Tsang, L.; Kong, J. A. Effective propagation constants for coherent electromagnetic wave propagation in media embedded with dielectric scatters. *J. Appl. Phys.* **1982**, *53*, 7162–7173.

(37) Varadan, V. K.; Bringi, V. N.; Varadan, V. V.; Ishimaru, A. Multiple scattering theory for waves in discrete random media and comparison with experiments. *Radio Science* **1983**, *18*, 321–327.

(38) Ding, K. H.; Tsang, L. Effective propagation constants of dense nontenuous media with multi-species of particles. *J. Electromag. Waves and Applications* **1986**, *2*, 757–777.

(39) Zhang, X.; Qiu, J.; Li, X.; Zhao, J.; Liu, L. Complex refractive indices measurements of polymers in visible and near-infrared bands. *Appl. Opt.* **2020**, *59*, 2337–2344.

(40) Nikolov, I. D.; Ivanov, C. D. Optical plastic refractive measurements in the visible and the near-infrared regions. *Appl. Opt.* **2000**, *39*, 2067–2070.

Appendix

A. Simple stray light model

We consider the standard transmission experiment for a sample with extinction OD E at a fixed wavelength. The incident intensity is I_0. The transmitted intensity is then

$$\bar{I}_t = I_0 10^{-E} + I_{\text{stray}}, \tag{12}$$

where I_{stray} represents the stray light at the fixed wavelength. If we define $p_S = I_{\text{stray}}/I_0$, we then have

$$\bar{I}_t = I_0 10^{-E} \left(1 + p_S 10^{E}\right), \tag{13}$$

The stray light also affect the reference measurement (typically water), for which we have

$$\bar{I}_t^{\text{ref}} = I_0 \left(1 + p_S\right), \tag{14}$$

The apparent (measured) extinction is then

$$E_m = E - \log_{10}\left(\frac{1 + p_S 10^{E}}{1 + p_S}\right) \tag{15}$$

As p_S is usually much smaller than one, this can be approximated as

$$E_m = E - \log_{10}\left[1 + p_S(10^{E} - 1)\right] \tag{16}$$

Note that in this simple model, p_S may in principle be wavelength-dependent.

B. Computing angular distributions for multiple scattering

The radiation profile for single scattering can be computed with Mie theory as explained in the main text. If we express it in terms of a probability distribution of the standard angles of scattering, θ and ϕ, we have:

$$p_1(\theta) = \frac{\pi F(\theta) \sin\theta}{\sigma_{\text{sca}}} \qquad [0 \leq \theta \leq \pi] \tag{17}$$

$$p_1(\phi) = \frac{1}{2\pi} \qquad [0 \leq \phi \leq 2\pi] \tag{18}$$

where the quantities have been defined earlier. Note that we are considering randomly polarized excitation, which removes any ϕ-dependence. Assuming we know the probability distribution of θ after exactly n scattering events, $p_n(\theta)$, we can then calculate $p_{n+1}(\theta)$ as follows.

- Choose a random angle θ_1 following the distribution $p_n(\theta)$ and a random ϕ_1. These characterize the direction $\mathbf{n}_1$ of the photon before $(n+1)$th scattering in the lab frame.
- Choose a random angle θ_2' following the single-scattering distribution $p_1(\theta)$ and a random ϕ_2'. These characterize the direction $\mathbf{n}_2$ of the photon after scattering, in the before-scattering photon frame (i.e. with respect to $\mathbf{n}_1$).
- Calculate the angle θ_2 of $\mathbf{n}_2$ in the lab frame. One can show that this is given by:

$$\cos\theta_2 = \sin\theta_2' \cos\phi_2' \sin\theta_1 + \cos\theta_2' \cos\theta_1. \tag{19}$$

- Repeat the previous steps for a large number of photons (5×10^6 in our case).
- Create a histogram of derived θ_2, which corresponds to the probability distribution $p_{n+1}(\theta)$.

$p_n(\theta)$ can therefore be computed iteratively from $p_1(\theta)$.

TOC Graphic

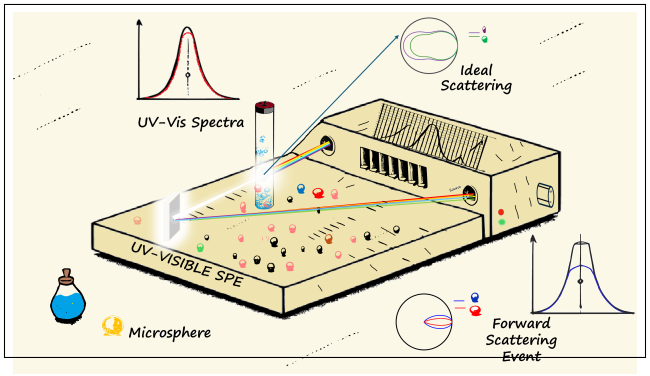
UV-Vis Spectra
Ideal Scattering
UV-VISIBLE SPE
Microsphere
Forward Scattering Event